Chapter 4

Ultrafast Nonlinear Optical Effects of Metal Nanoparticles Composites

Kwang-Hyon Kim, Anton Husakou and Joachim Herrmann

Additional information is available at the end of the chapter

http://dx.doi.org/10.5772/67412

Abstract

We present a theoretical method for the calculation of the transient nonlinearity in dielectric composites doped with metal nanoparticles and demonstrate some applications of this approach. First, we describe the theoretical basis of the linear and nonlinear properties of metal nanoparticles by using the time-domain discrete-dipole approximation. By using the two-temperature model for the description of the electron-electron and electron-lattice interaction, we derive an equation for the transient third-order nonlinear susceptibility. Based on this method and the effective medium approximation, we present numerical results for the nonlinear optical susceptibility for different nanocomposites media consisting of noble metal nanoparticles surrounded by a dielectric host. With increasing pump intensities, the plasmon resonance is shifted which leads to a saturation of the absorption. We present a theory of mode-locking of solid-state and semiconductor disk lasers using metal nanocomposites as saturable absorbers. Finally, we consider a novel slow-light device based on metal nanocomposites.

Keywords: metal nanoparticles, nanocomposite materials, nonlinear optical response, third-order nonlinear susceptibility, time-domain discrete-dipole approximation, effective medium approximation, saturation of absorption, mode-locking of lasers, slow light

1. Introduction

Metal nanoparticles (NPs) play a key role in the emerging field of nanooptics and plasmonics. The interaction between light and metal NPs is determined by charge-density oscillations on the surface of the particles, or so-called localized plasmon resonances. These elementary electronic excitations have been extensively studied, both in fundamental direction and with

a view to applications (for reviews see e.g., Refs. [1–3]). Examples of the diverse fields of applications include localized plasmons, which allow greatly increased signal strengths in Raman spectroscopy and surface spectroscopy, significant enhancement of the emission rate of fluorescent molecules or quantum dots, increased efficiency and brightness of light-emitting devices (LEDs), as well as novel forms of fluorescence microscopy. The plasmonic properties of nanoparticles exhibit a highly sensitive dependence on its shape, and the plasmonic resonance is shifted in nonspherical particles, especially rods, spheroids, triangular prisms or bow-tie antennas to longer wavelengths [4].

The huge nonlinearity of metallic nanostructures after intense excitation with fs laser pulses is related to the response of intraband and interband nonlinear electronic processes to the electromagnetic field. Early theoretical studies of the Kerr-type nonlinear susceptibilities in composite media are reported in Refs. [5–7]. A review of main results can be found in Ref. [8]. More recently using the discrete-dipole approximation, linear and nonlinear optical characteristics of metal composites with nanoparticles with different sizes and shapes have been studied in Refs. [9–11], and the saturation of absorption in such materials in Ref. [12].

In Section 2 of this chapter, we present a method for the calculation of the linear and nonlinear properties of metal nanoparticles by using the time-domain discrete-dipole approximation and derive an equation for the transient nonlinear susceptibility based on the two-temperature model for the description of the electron-electron and electron-lattice interaction. In Section 3, we present numerical results for the ultrafast third-order nonlinear optical susceptibility for different nanocomposites media consisting of a noble metal nanoparticles surrounded by a dielectric host. Based on the predicted saturable absorption in Section 4, we describe ultrashort pulse generation by mode-locking of short-wavelength solid-state and semiconductor disk lasers using metal nanocomposites. In Section 5, we describe a mechanism for the realization of slow light phenomenon by using glasses doped with metal nanoparticles in a pump-probe regime near the plasmonic resonance due to the sensitive frequency dependence of the refractive index related with the saturable absorption [13].

2. Theoretical fundamentals

In this section, we introduce the basic theoretical model for ultrafast nonlinear optical responses of dielectric composites containing metal nanoparticles based on the time-domain discrete-dipole approximation and the two-temperature model.

2.1. Time-domain discrete-dipole approximation for the calculation of the ultrafast nonlinear optical responses of composites containing metal nanoparticles with different sizes and shapes

To evaluate the change of the dielectric function of metals, we should obtain the distribution of the amplitude of the enhanced field $A_{\mathrm{enh}}(t)$ in metal NPs. The popular numerical method for calculating the transient field distribution in NPs is the finite-difference time-domain (FDTD) method. However, for the evaluation of the ultrafast nonlinear change of the dielectric function of a metal, we should know the amplitude $A_{\mathrm{enh}}(t)$ which requires very significant

http://dx.doi.org/10.5772/67412

computational effort with FDTD. For the evaluation of $A_{\mathrm{enh}}(t)$, we use the time-domain discrete-dipole approximation (TDDDA) [10, 11]. Below, we briefly describe the basics of this numerical approach.

TDDDA is a numerical tool for evaluating the distribution of amplitude of real or enhanced field in metal NPs with arbitrary sizes and shapes. It is a time-domain version of conventional frequency-domain discrete-dipole approximation (DDA). TDDDA describes NPs as the collection of small dipoles. The amplitude $\mathbf{A}_m$ of the enhanced field at the m-th dipole is given by the following integral-differential equation:

$$\mathbf{A}_m = \left(1 - \frac{\varepsilon_{\mathrm{h}}^{1/2}}{c_0} r_{m\perp} \frac{\partial}{\partial t} + \frac{\varepsilon_{\mathrm{h}}}{2c_0^2} r_{m\perp}^2 \frac{\partial^2}{\partial t^2}\right) \mathbf{A}_m^{\mathrm{in}} e^{\mathrm{i}k_0 r_{m\perp}} + \left\{-\frac{4\pi}{3} + \sum_{n\neq m}\left[G_{mn}^{(0)} + \mathrm{i}G_{mn}^{(1)} \frac{\partial}{\partial t} - G_{mn}^{(2)} \frac{\partial^2}{\partial t^2}\right] v\right\} \mathbf{Q}_n, \tag{1}$$

where ε_h is the permittivity of the host medium, c_0 is the light velocity in vacuum, $\mathbf{A}_m^{\mathrm{in}}$ and $\mathbf{Q}_m$ are the amplitudes of the incident field and polarization at the place of the m-th dipole, $r_{m\perp} = (\mathbf{k}\cdot\mathbf{r}_m)/k$ is the projection of $\mathbf{r}_m$ onto the direction of wavevector $\mathbf{k}$ of incident pulse, with $\mathbf{r}_m$ being the position vector at m-th dipole. In Eq. (1), $\mathbf{G}_{mn}^{(0)}$, $\mathbf{G}_{mn}^{(1)}$, and $\mathbf{G}_{mn}^{(2)}$ are tensors given by

$$\mathbf{G}_{mn}^{(0)} = \frac{\exp(\mathrm{i}k_0 R_{mn})}{R_{mn}} \left[k_0^2(\mathbf{1} - \hat{r}_{mn} \otimes \hat{r}_{mn}) + \frac{\mathrm{i}k_0 R_{mn} - 1}{R_{mn}^2}(\mathbf{1} - 3\hat{r}_{mn} \otimes \hat{r}_{mn})\right],$$

$$\mathbf{G}_{mn}^{(1)} = \frac{\varepsilon_{\mathrm{h}}^{1/2}}{c_0} \frac{\exp(\mathrm{i}k_0 R_{mn})}{R_{mn}} [k_0(2 + \mathrm{i}k_0 R_{mn})(\mathbf{1} - \hat{r}_{mn} \otimes \hat{r}_{mn}) - k_0(\mathbf{1} - 3\hat{r}_{mn} \otimes \hat{r}_{mn})],$$

$$\mathbf{G}_{mn}^{(2)} = \frac{\varepsilon_{\mathrm{h}}}{2c_0^2} \frac{\exp(\mathrm{i}k_0 R_{mn})}{R_{mn}} [(-k_0^2 R_{mn}^2 + 4\mathrm{i}k_0 R_{mn} + 2)(\mathbf{1} - \hat{r}_{mn} \otimes \hat{r}_{mn}) - (\mathrm{i}k_0 R_{mn} + 1)(\mathrm{i}k_0 R_{mn} + 1)], \tag{2}$$

where $k_0 = \omega_0/c_0$ is the wave number at the central angular frequency ω_0 of incident light pulse, $R_{mn} = |\mathbf{r}_m - \mathbf{r}_n|$, $\hat{r}_{mn} = (\mathbf{r}_m - \mathbf{r}_n)/R_{mn}$. The amplitude of the polarization $\mathbf{Q}_m(t)$ in Eq. (1) is determined by $\mathbf{Q}_m = \beta \mathbf{A}_m + \mathbf{Q}_{m1}$, where $\beta = [(\varepsilon_\infty/\varepsilon_{\mathrm{h}}) - 1]/(4\pi)$, ε_∞ is the dielectric function for infinite frequency. In this formalism, we use the extended Drude model for the linear dielectric function of a metal given by $\varepsilon_{\mathrm{m0}} = \varepsilon_\infty - \omega_{\mathrm{p}}^2/(\omega^2 + i\gamma\omega)$, where ω_{p} is the plasma frequency, and γ is the electron collision frequency. In the equation for $\mathbf{Q}_m$, $\mathbf{Q}_{m1}$ is determined by

$$\ddot{\mathbf{Q}}_{m1} + c\dot{\mathbf{Q}}_{m1} + b\mathbf{Q}_{m1} = a\mathbf{A}_m, \tag{3}$$

where $a = \omega_{\mathrm{p}}^2/(4\pi\varepsilon_{\mathrm{h}})$, $b = -(\omega_0^2 + \mathrm{i}\gamma\omega_0)$, and $c = \gamma - 2\mathrm{i}\omega_0$. The basic principle of TDDDA and the detailed derivations of the above equations can be found in Ref. [10].

2.2. Transient nonlinear Kerr-type optical nonlinearity

The transient nonlinear optical response of metal NPs is related with the electron and phonon temperatures. Upon illuminating metal nanoparticles, femtosecond laser pulses excite the

nonequilibrium electron distribution and thermalization process follows through the interactions between electrons. The time scale of electron-electron interactions τ_{ee} is about a few hundreds femtoseconds. The electron system transfers its energy to the lattices through electron-phonon coupling, the time scale τ_{ep} of which is a few picoseconds. The thermalized part of electrons, in part, is cooled through heat exchange with lattices in the NPs. The above outlined processes can be described by the following phenomenological rate equations (see e.g., Refs. [14, 15]):

$$\begin{aligned} \frac{\partial N}{\partial t} &= -\frac{N}{\tau_{ee}} - \frac{N}{\tau_{ep}} + \delta P(t), \\ C_e \frac{\partial T_e}{\partial t} &= -G(T_e - T_L) + \frac{N}{\tau_{ee}}, \\ C_L \frac{\partial T_L}{\partial t} &= G(T_e - T_L) + \frac{N}{\tau_{ep}}, \end{aligned} \tag{4}$$

where N is the energy density stored in the nonthermalized part of the distribution; $P(t)$ is the absorbed laser power per unit volume; δ is a constant representing the contribution of light field to the generation of excited nonequilibrium electrons; C_e and C_L are the heat capacities, C_e and C_L are the temperatures of electrons and lattices, respectively; G is the cooling time constant.

The above rate equations describe only the temperatures of thermalized electrons and lattices. The relations between the optical responses of metal nanoparticles and these temperatures can be found by the following considerations. The change of transient transmittance ΔT, an experimentally observable nonlinear quantity, is a linear function of the dielectric function of NPs [14]:

$$\frac{\Delta T}{T} = \frac{\partial lnT}{\partial \varepsilon_1}\Delta\varepsilon_1 + \frac{\partial lnT}{\partial \varepsilon_2}\Delta\varepsilon_2, \tag{5}$$

where T is the transmittance of the composite, ε_1 and ε_2 are real and imaginary parts of the dielectric functions of metal, and Δ represents the change of the corresponding quantities. The change of dielectric functions depends on redistribution of the electron energy in the vicinity of the Fermi level. Such a change can be accurately described by a linear function of the electronic and lattice temperatures [14] in the case of weak pump energy and the above equation can be represented as

$$\frac{\Delta T}{T} = aT_e(t) + bT_L(t), \tag{6}$$

where a and b are constants.

From Eqs. (5) and (6), we can conclude that, in the considered case, the change of dielectric function of metal is proportional to the change of electronic and lattice temperatures. The empirical results show, however, that the influence of lattice temperature on the dielectric function change is negligible. From these facts, the change of the dielectric function of a metal $\Delta\varepsilon_m$ can be written [16]:

$$\Delta\varepsilon_m(t) = \eta\Delta T_e, \tag{7}$$

where η is a constant.

http://dx.doi.org/10.5772/67412

The disadvantage of this model is that it cannot directly account for the nonlinear optical parameters such as nonlinear refractive index and absorption. To solve this problem, below we relate the unknown parameters in Eqs. (4) and (7) with the nonlinear optical susceptibility of the metal which can be experimentally determined.

From the second and the third equations in Eq. (4), we obtain

$$\frac{\partial(T_e - T_L)}{\partial t} = -G\left(\frac{1}{C_e} + \frac{1}{C_L}\right)(T_e - T_L) + \left(\frac{1}{C_e\tau_{ee}} - \frac{1}{C_L\tau_{ep}}\right)N. \tag{8}$$

Introducing the cooling time $\tau_{ep} = C_eC_L/[G(C_e + C_L)]$ and taking into account that the increase of lattice temperature can be neglected compared to that of electrons and $T_e - T_L \approx T_e - T_0$, we obtain

$$\frac{\partial(T_e - T_0)}{\partial t} = -\frac{T_e - T_0}{\tau_{ep}} + \left(\frac{1}{C_e\tau_{ee}} - \frac{1}{C_L\tau_{ep}}\right)N, \tag{9}$$

where T_0 is the initial temperatures of electrons and lattices. On the other hand, integrating the first equation in Eq. (7) we have

$$N = \delta\int_{-\infty}^{t} P(t')exp\left(-\frac{t-t'}{\tau_{ee}'}\right)dt', \tag{10}$$

where $\tau_{ee}'^{-1} = \tau_{ee}^{-1} + \tau_{ep}^{-1}$. Combining Eqs. (9) and (10), we obtain

$$\frac{\partial(T_e - T_0)}{\partial t} = -\frac{T_e - T_0}{\tau_{ep}} + \delta\left(\frac{1}{C_e\tau_{ee}} - \frac{1}{C_L\tau_{ep}}\right)\int_{-\infty}^{t} P(t')exp\left(-\frac{t-t'}{\tau_{ee}'}\right)dt'. \tag{11}$$

From Eq. (7),

$$\frac{\partial\Delta\varepsilon_m}{\partial t} = \eta\frac{\partial(T_e - T_0)}{\partial t}. \tag{12}$$

By using Eqs. (11) and (12), we can write

$$\frac{\partial\Delta\varepsilon_m}{\partial t} = -\frac{\Delta\varepsilon_m}{\tau_{ep}} + \delta'\left(\frac{1}{C_e\tau_{ee}} - \frac{1}{C_L\tau_{ep}}\right)\int_{-\infty}^{t} P(t')exp\left(-\frac{t-t'}{\tau_{ee}'}\right)dt', \tag{13}$$

where ε_m is the dielectric function of metal as a function of time and incident intensity, and $\delta' = \eta\delta$. The absorbed energy density $P(t)$ must be proportional to the enhanced intensity in the metal NPs and therefore we find

$$\frac{\partial\Delta\varepsilon_m}{\partial t} = -\frac{\Delta\varepsilon_m}{\tau_{ep}} + \frac{\beta}{\tau_{ee}}\int_{-\infty}^{t} |A_{enh}(t')|^2 exp\left(-\frac{t-t'}{\tau_{ee}'}\right)dt', \tag{14}$$

where β is a constant proportional to $\delta'[C_e^{-1} - C_L^{-1}(\tau_{ee}/\tau_{ep})]$ and $A_{enh}(t)$ is the amplitude of enhanced field. To determine the constant β, we consider the steady-state nonlinear solution of

Eq. (14). For a steady-state pumping, Eq. (14) gives $\Delta\varepsilon_{\mathrm{m,\,static}} = \beta\tau_{\mathrm{ep}}|A_{\mathrm{enh}}|^2$ and we have $\beta = \chi_{\mathrm{m}}^{(3)}/\tau_{\mathrm{ep}}$, where $\chi_{\mathrm{m}}^{(3)}$ is the inherent degenerate third-order susceptibility of the metal. Consequently, we obtain [17]

$$\frac{\partial\Delta\varepsilon_{\mathrm{m}}}{\partial t} = -\frac{\Delta\varepsilon_{\mathrm{m}}}{\tau_{\mathrm{ep}}} + \frac{\chi_{\mathrm{m}}^{(3)}}{\tau_{\mathrm{ee}}\tau_{\mathrm{ep}}}\int_{-\infty}^{t}|A_{\mathrm{enh}}(t')|^2 exp\left(-\frac{t-t'}{\tau_{\mathrm{ee}}'}\right)dt', \tag{15}$$

Since the pure e-e scattering time τ_{ee} (typically around 100 fs) is much shorter than τ_{ep} (typically around or longer than 1 ps), in Eq. (15), τ_{ee}'can be replaced with τ_{ee}. The resultant dielectric function is determined by ε_{m}= $\varepsilon_{\mathrm{m0}}$ + Δ $\varepsilon_{\mathrm{m}}(t)$, where $\varepsilon_{\mathrm{m0}}$ is the linear dielectric function of metal.

Equation (15) is the major governing equation for the ultrafast nonlinear optical responses of metal nanoparticles.

3. Numerical results for the ultrafast nonlinear response of metal NPs composites

3.1. The effective medium approximation

The transient distribution of the amplitude $\mathbf{A}_m$ obtained by using Eq. (1) is used for the calculations of the distribution of the nonlinear dielectric function $\varepsilon_n^{\mathrm{NL}}$ in metal nanoparticles, on each time step by using Eq. (15). The effective nonlinear dielectric function of the metal nanocomposite is calculated by using the effective medium approximation (EMA) $\varepsilon_{\mathrm{eff}}^{\mathrm{NL}} = \langle\varepsilon A\rangle/\langle A\rangle$ [9], where the average is done over the distribution of dipoles and A is, the amplitude of the enhanced field. In the calculations based on EMA, the dielectric function ε and the field amplitude A in the nanoparticle region are $\varepsilon_{\mathrm{m},n}^{\mathrm{NL}}$ (subscription m represents metal and n denotes the value at n-th dipole) and the enhanced field A_m calculated with the TDDDA. In the spatial areas outside of the nanoparticles, we take the permittivity of the host ε_{h} as ε and the amplitude of incident field as A. The volume of host medium is calculated using the filling factor f, which is the volume ratio of metal NPs to the volume of the host medium. After obtaining the effective nonlinear dielectric function of metal nanocomposite $\varepsilon_{\mathrm{eff}}^{\mathrm{NL}}$, one can calculate the nonlinear optical characteristics such as the nonlinear effective index and absorption coefficient. The effective refractive index of the composites is determined by $n_{\mathrm{eff}}^{\mathrm{NL}} = \mathrm{Re}\sqrt{\varepsilon_{\mathrm{eff}}^{\mathrm{NL}}}$. The nonlinear effective absorption coefficient of the composite is given by $\alpha_{\mathrm{eff}}^{\mathrm{NL}} = 2(c_0/\omega_0)\mathrm{Im}\sqrt{\varepsilon_{\mathrm{eff}}^{\mathrm{NL}}}$ and the transmittance by $T^{\mathrm{NL}} = \exp(-\alpha_{\mathrm{eff}}^{\mathrm{NL}}l)$, where l is the thickness of the composite film. Then, the relative change of transmittance $\Delta T/T$ is calculated by $(T^{\mathrm{NL}}-T^{\mathrm{L}})/T^{\mathrm{L}}$, where T^{L} is the linear transmittance.

For the special case of very small and spherical NPs, the amplitude of the enhanced field can be approximately calculated by $A_{\mathrm{enh}}(t) = x(t)A_0(t)$, where $x(t) = \varepsilon_{\mathrm{h}}/[\varepsilon_{\mathrm{m}}(t) + 2\varepsilon_{\mathrm{h}}]$ is the transient field enhancement factor and A_0 is the amplitude of the incident pump pulse. The nonlinearly

modified $\varepsilon_m(t)$ is self-consistently calculated in combination with the above-mentioned enhanced amplitude $A_{enh}(t)$. The resultant effective dielectric function of the composite ε_{eff}^{NL} is calculated by using Maxwell-Garnett model.

3.2. Numerical results and discussions

In this section, we present the numerical results for the ultrafast nonlinear optical responses of metal NPs composites.

Figure 1 shows an example of the time-dependent nonlinear transmission of a metal nanocomposite. The figure shows $\Delta T/T$ of a 0.2-μm-thick Al_2O_3 film doped with Ag NPs. We consider NPs with diameter of 6.5 nm, and a filling factor of 1%. The value of pump fluence is assumed to be 100 μJ/cm^2. For the optimal fit with the experimental data [18], we use the e-e and cooling times of τ_{ee} = 100 fs and τ_{ep} = 0.70 ps, correspondingly. Though the pump pulse is in the sub-100 fs range, the transmittance responds slower, which is explained by the delayed thermalization of electrons. In both cases, the time necessary to reach a maximum change in the transmittance is roughly 200–250 fs longer than the e-e scattering time τ_{ee}. The exponential decay of the transmittance change depends on the cooling time τ_{ep} and also on the pump fluence. Here we assume for the two response times τ_{ee} = 100 fs and τ_{ep} = 1 ps.

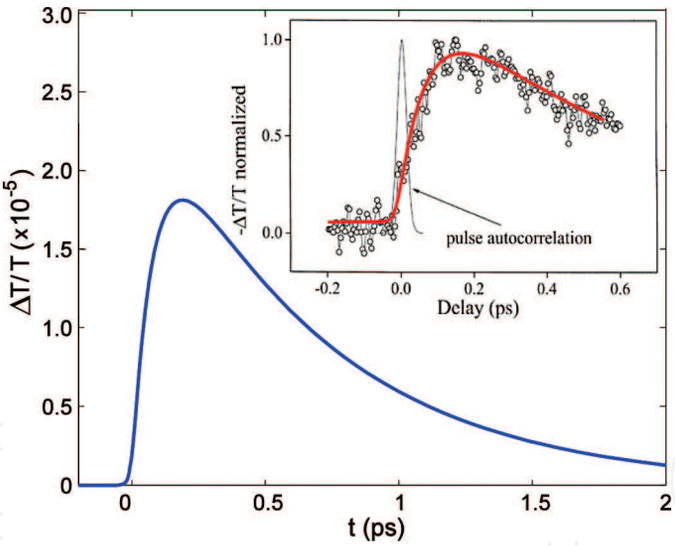

Figure 1. The transient nonlinear absorption of metal nanocomposites in an alumina film containing Ag NPs with filling factor of 1% and with particles diameter of 6.5 nm. The pump and probe have the central wavelength of 800 nm and 30 fs. We consider 0.25-μm-thick composite film. In the inset, the experimental (points, from Ref. [18]) and the theoretical (solid curve) results are compared.

Figure 2 presents the transient behavior of the effective refractive index (a) and the transmittance (b) of a 1-μm-thick silica glass layer doped with very small Ag nanospheres at pump light at 430 nm. In **Figure 2**, one can see that the relaxation of the transmittance is slower for a higher fluence of the incident light even for a fixed value of inherent cooling time of silver as large as 1 ps.

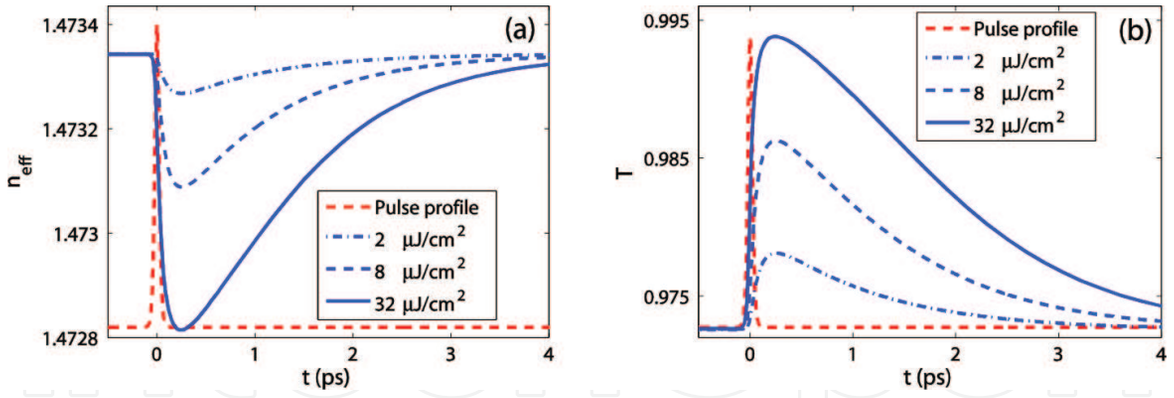

Figure 2. Refractive index (a) and transmittance (b) of silica glass doped with Ag NPs with diameters below 10 nm for different fluences of 50 fs pulses at 430 nm. Filling factor is 10^{-4} and thickness is considered to be 1 μm. The red-dashed curves in both panels represent the temporal profile of the pump pulse.

To investigate the dependence on the NP shape, we numerically investigate the ultrafast nonlinear responses of composites containing nonspherical metal nanoparticles, considering silica glass doped with silver nanorods. To study the dependency of the ultrafast nonlinear responses on the aspect ratio, we have taken nanorods with constant volumes. Note that the quantities presented in **Figures 3(a)** and **(b)** have been averaged over the possible polarization directions versus the orientations of nanorods. For the simulations, we have taken nanorods with different aspect ratio and geometry, as indicated in the figure. **Figure 3(a)** illustrates extinction spectra of silver nanorods with different aspect ratios, embedded in silica. As the figure shows, nanorod with a larger value of the aspect ratio (length divided by the diameter) exhibits surface plasmon resonance (SPR) at a longer wavelength. The main SPR peaks appear at 595, 680, and 800 nm for silver nanorods with aspect ratio of 1.68, 2.25, and 3.11, respectively. These peaks represent dipole plasmonic resonances for the case when the axes of nanorods are parallel to the polarization of incident light. The minor SPR peaks, which correspond to the dipole resonances for the polarization direction of incident wave perpendicular to the axes of nanorods, also appear

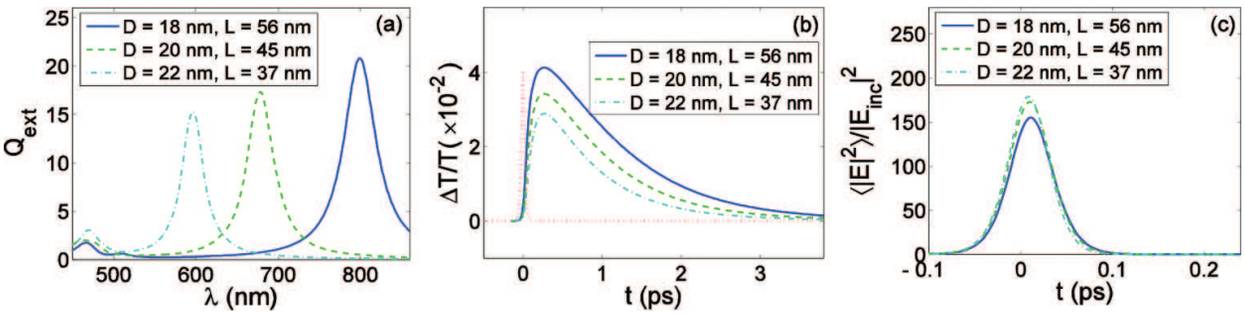

Figure 3. Ultrafast nonlinear response of silica glasses doped with silver nanorods with varying shape. The diameters D and the lengths L of nanorods are given in insets. The volumes of silver nanorods are kept the same for all the aspect ratios. Filling factor is 10^{-4} and the thickness of composite film is assumed to be 1 μm. (a) shows extinction spectra and (b) depicts the nonlinear change of relative transmittance $\Delta T/T$ for the different shapes of silver nanorods at the wavelengths corresponding to the main SPR peaks. The quantities shown in (a) and (b) are averaged over all the possible polarization directions relative the orientations of nanorods. Pulse duration and the fluence are taken to be 50 fs and 2 μJ/cm^2, respectively. In (b), red-dotted curve shows the temporal profile of incident pump pulse. (c) shows the space-averaged intensity enhancement when the axes of nanorods are parallel to the polarization of pump pulse.

(at around 470 nm). **Figure 3(b)** illustrates the nonlinear change of relative transmittance $\Delta T/T$ for the different aspect ratios of silver nanorods at the wavelengths corresponding to the main SPR peaks. The figure also shows that the maximum change of $\Delta T/T$ becomes larger for the nanorod with larger aspect ratio. We can expect that the stronger nonlinear response originates from a stronger intensity enhancement in the silver nanorod, which we can confirm from **Figure 3(c)**.

With the theoretical tool for calculation of the ultrafast nonlinear optical responses of metal NPs composites, below we theoretically demonstrate its possible use for the mode-locking and slow light devices by using these materials.

4. Ultrashort pulse generation by mode-locking of lasers using metal nanocomposites as saturable absorbers

In this section, we present the theory of mode-locking of visible solid-state [13] and semiconductor disk lasers [17] using metal nanocomposites as saturable absorbers.

4.1. Mode-locking of solid-state lasers

In this subsection, we present the general passive mode-locked operation of solid-state lasers taking Ho:YLF laser pumped with a diode laser as an example and a metal nanocomposite as saturable absorber.

The master equation for mode-locking of solid-state lasers can be written as follows [19]:

$$T_{\mathrm{R}}\frac{\partial A(T,t)}{\partial T} = -iD\frac{\partial^2 A}{\partial t^2} + i\delta|A|^2A + \left[g - l + D_{\mathrm{g,f}}\frac{\partial^2 A}{\partial t^2} - q(T,t)\right]A(T,t), \tag{16}$$

where D is the second-order intracavity group delay dispersion (GDD), $D_{\mathrm{g,f}} = g/\Omega_{\mathrm{g}}^2 + 1/\Omega_{\mathrm{f}}^2$ the gain and intracavity filter dispersion, Ω_{g} and Ω_{f} are the gain and filter bandwidth, respectively. The coefficient $\delta = (2\pi/\lambda_0 A_{\mathrm{L}})n_2 l_{\mathrm{L}}$ represents the nonlinear effect by the Kerr nonlinearity in the gain crystal leading to self-phase modulation (SPM), where λ_0 is the central lasing wavelength, n_2 is the nonlinear index of laser active medium, A_{L} and l_{L} are the effective mode area and optical pass per round-trip. The gain coefficient is given by $g = g_0/[1 + E/(P_{\mathrm{L}}T_{\mathrm{R}})]$, where g_0 is the small-signal gain, E is the pulse energy, P_{L} is the saturation power of laser material, l is the linear loss inherent to the passive resonator, and q is the loss by saturable absorber.

As an example, we investigate the mode-locking of a Ho:YLF laser operating at 545 nm and pumped at 445 nm which contains SCHOTT glass N-BAK 4 doped with Au NPs (with filling factor 2×10^{-3}). In such a case, the laser gain medium functions as a three-level system [20]. The Ho:YLF crystal has an emission linewidth of roughly 18 nm and a strong absorption peak around 450 nm which can be used for pumping with high power laser diodes. We have assumed the absorption cross sections at 445 and 545 nm to be 3×10^{-21} cm^2 and 5×10^{-21} cm^2,

correspondingly, emission cross section at 545 nm to be 8×10^{-21} cm^2 [21], and the fluorescence lifetime of 110 μs [21]. The lasing transition corresponds to ${}^5S_2-{}^5I_8$ [20]. For the Ho^{3+} concentration of 1.2×10^{20} cm^{-3}, a beam area on the crystal with 1000 μm^2, a pump intensity 0.6 MW/cm^2 corresponding to a pump power of 6 W, a crystal length of 10 mm, and a resonator length of 1 m corresponding to a repetition rate of 0.15 GHz, we have the main laser parameters of g_0 = 0.22, P_L = 4.69 W, Ω_g = 57.08 THz, and δ = 3.94 MW^{-1}. We assumed the passive resonator loss to be l = 0.02. As the saturable absorber for passive mode-locking, we consider a metal nanocomposite given by a layer of SCHOTT glass (N-BAK 4) doped with small Au NPs. The plasmon resonance is found at 543 nm and we expect strong saturable absorption since the plasmon resonance peak is located near the central lasing wavelength. The saturable absorber loss is determined by $q(t) = -i(\omega/c)\sqrt{\varepsilon_{\text{eff}}(t)}d$, where ω is central frequency, and d is the thickness of metal nanocomposite absorber. The cross section of beam on the metal nanocomposite absorber is taken to be 0.01 mm^2.

Figure 4 presents results for the passive mode-locking behavior of a Ho:YLF laser obtained by the solution of Eq. (16). Here, the GDD parameter has a value of −20 fs^2. As **Figure 4(a)** shows, the pulse duration rapidly decreases during the early stage of mode-locking and it is then stabilized.

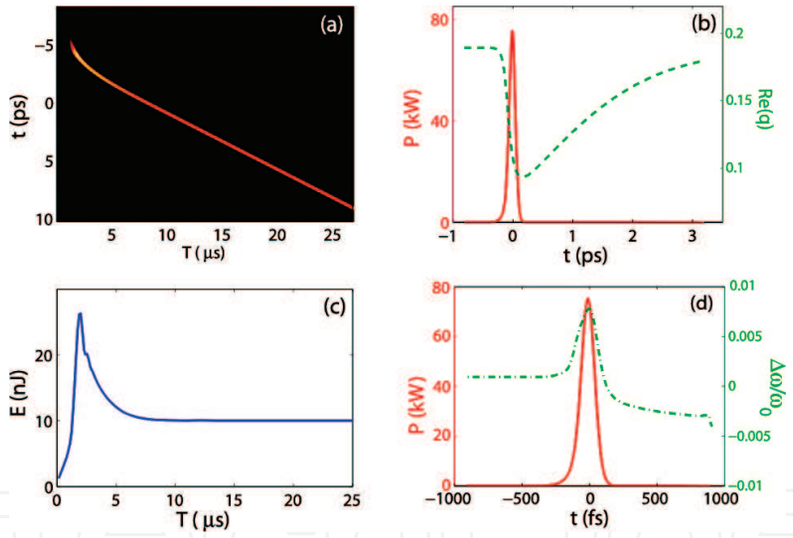

Figure 4. Mode-locking of Ho:YLF laser with SCHOTT glass N-BAK 4 doped with small Au NPs: (a) pulse evolution, (b) pulse profile and the dynamics of absorber loss, (c) evolution of pulse energy, and (d) intensity and frequency profile. D = −10 fs^2.

The numerical results show that the shortest pulse duration of about 100 fs is much smaller than the recovery time of 1 ps. In the early time of femtosecond pulse generation in solid-state lasers by the use of saturable absorbers for passive mode-locking, it was believed that the shortest pulse duration cannot be smaller than the recovery time of the absorber. However, due to the combined influence of spectral broadening by SPM and GVD, a slow response of the absorber with a recovery time larger than the pulse duration is sufficient for mode-locking [22, 23]. Pulse stabilization and shaping mechanism in this case can be explained by the fact that the action of the absorber steadily delays the pulse, similar as in solid-state lasers mode-

http://dx.doi.org/10.5772/67412

locked by a semiconductor saturable absorber [24, 25]. Thus, the pulse moves slower than any noise structure behind the pulse maximum, and therefore, it fuses with the main pulse before it experiences high enough gain. This behavior is illustrated in **Figure 4(b)**.

Figure 5 shows results for the dependences of pulse duration and energy on the parameters of the laser.

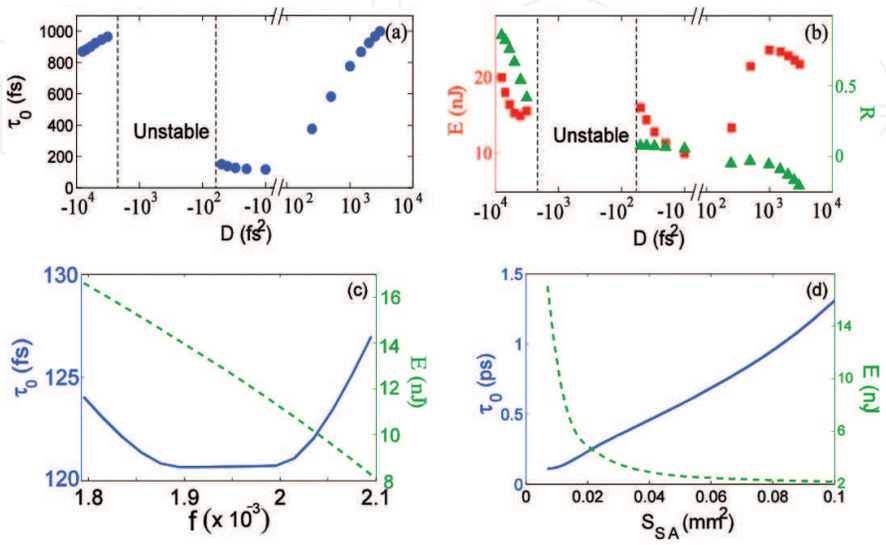

Figure 5. Dependence of pulse duration (a), energy [red squares in (b)], and the ratio R [green triangles in (b)] on the GDD parameter D. The beam area on the metal nanocomposite is 0.01 mm^2 and filling factor is 2×10^{-3}. (c) presents the dependences of pulse duration and pulse energy on filling factor. The beam area on the metal nanocomposite is 0.01 mm^2 and $D = -20$ fs^2. (d) depicts the dependencies of pulse duration and energy, and the ratio R on the beam area on the metal nanocomposite saturable absorber: $D = -20$ fs^2 and $f = 2 \times 10^{-3}$.

The resonator dispersion (the GDD parameter) is one of the key parameters affecting the mode-locking stability, pulse duration as well as energy. The simulations predict that the pulse evolution is unstable for the GDD parameter D from -55 fs^2 up to around -3200 fs^2 for the other parameters equal to those in the above subsections. The physical mechanism of the instability is the imbalance between the pulse delay, originating from the delayed absorber response in the metal nanocomposite, and pulse reshaping by the dispersion. In **Figure 5**, we show the dependence of the pulse duration and energy on the intracavity dispersion for a filling factor of 2×10^{-3}. As the dispersion increases, the pulse duration increases as well, independent of the sign of dispersion.

Figure 5(c) depicts the dependences of pulse duration and energy on the filling factor for $D = -20$ fs^2 and the beam area on the metal nanocomposite. For a small filling factor, we find a small maximum loss change leading to a larger pulse duration. For a filling factor smaller than 1.7×10^{-3}, mode-locking becomes unstable. For a filling factor larger than 2.1×10^{-3}, the total linear loss introduced by the saturable absorber is higher than the gain and the lasing itself becomes impossible.

In **Figure 5(d)**, pulse duration and energy are presented in dependence on the beam area for the metal nanocomposite absorber film with $D = -20$ fs^2 and $f = 2 \times 10^{-3}$. In the figure, the mode-locking process is stable for the beam area larger than 0.1 mm^2 or smaller than 6000 μm^2.

The pulse duration increases as the beam area increases, caused by the change of the reduced maximum. The possible duration range is from 110 fs to 1.31 ps. The shortest pulse duration of 100.7 fs is predicted for $D = 0$, beam area 6000 μm^2, and filling factor 2×10^{-3}.

Mode-locking of solid-state lasers by a slow absorber but shaped by the interplay between negative group-delay dispersion and SPM is often interpreted by the mechanism of soliton mode-locking, where the pulse is completely shaped by soliton formation and the saturable absorber only stabilizes the soliton against the growth of noise [23]. Whether such regime is indeed realized can be estimated by the ratio $R = -8ln(\sqrt{2}+1)D/(\delta E\tau_0)$, where τ_0 is the pulse duration full width at half maximum (FWHM). If the value of R is equal to 1, the pulse formation mechanism can be interpreted by soliton mode-locking. In **Figure 5(b)**, the ratio R is depicted by the green triangles. As can be seen in the left stability range, the factor R is in the range of 0.5, while in the right stability range, R is near zero. This means the predicted mode-locking behavior cannot be interpreted by the mechanism of soliton mode-locking, and in contrast to this interpretation, the action of the saturable absorber influences the pulse parameter. This is also confirmed by the calculated frequency chirp in **Figure 5(d)** which is not zero unlike that of a soliton. Note that the very specific regime of soliton mode-locking is not requested and femtosecond pulse generation in solid-state lasers by slow absorbers can be achieved under more general conditions [22].

4.2. Mode-locking of semiconductor lasers

Here, we investigate the possibility of femtosecond pulse generation by mode-locking of semiconductor disk lasers (SDLs) in visible range by using of metal nanocomposites as slow saturable absorbers. In contrast to the solid-state gain media, the semiconductors exhibit a dynamic gain in one round trip of the pulse in the resonator. This characteristic makes the process quite different from the mode-locked solid-state lasers but similar to one in passively mode-locked dye lasers. Mode-locking in this case rely on the interplay between a slow saturable absorber and slow gain saturation, which opens a net gain window in time, so that the pulse itself experiences gain per round trip and noise is discriminated outside this net gain window.

Passively mode-locked operation of the SDLs is described by the following master equation:

$$T_R \frac{\partial A(T,t)}{\partial T} = -iD\frac{\partial^2 A}{\partial t^2} + \left[(1-i\alpha)g - l + D_{g,f}\frac{\partial^2 A}{\partial t^2} - q(T,t)\right]A(T,t), \tag{17}$$

where α is the linewidth enhancement factor [26, 27]. In the above equation, the gain coefficient $g(t)$ is given by [26]

$$\frac{\partial g(t)}{\partial t} = -\frac{g(t)-g_0}{\tau_g} - g(t)\frac{|A(t)|^2}{E_g}, \tag{18}$$

where τ_g is the gain recovery time and E_g is the gain saturation energy dependent on the saturation fluence and the beam diameter on the gain medium. The temporal dynamics of the gain leads to a depletion of the leading edge of pulse which is absent in the case of solid-state lasers due to the quasi-static gain. On the other hand, the slow saturable nanocomposite

absorber suppresses the trailing edge, and the combined action of both creates a net gain window with negative gain both on the leading and the trailing front of the generated pulse.

As an example, we consider a GaN-based SDL [27] operating with a central lasing wavelength of 420 nm. The small signal gain is chosen to be $g_0 = 2$, the gain linewidth $\Omega_g = 2\pi \times 20.39$ THz, the linewidth enhancement factor $\alpha = 2.8$ Lu et al. [27], the gain recovery time to be 1 ns [28], and the saturation energy for the gain medium to be 0.6 nJ. As a saturable absorber, we consider a silica glass film doped with Ag nanospheres with diameters smaller than 10 nm. The filling factor is taken to be 7×10^{-3}. In this case, the plasmon resonance is located at 414 nm and the composite exhibits strong saturated absorption near 420 nm.

In **Figure 6**, we present an example of passively mode-locked operation of this laser with a cavity dispersion of $D = 100$ fs^2 and a beam area on the metal nanocomposite of 0.002 mm^2. As can be seen in Figures 6(a) and (c) in this case, pulse shortening happens in the very beginning of the process up to about 20 ns, while the stabilization is achieved after about ~200 ns and is faster than in solid-state lasers (several μs). **Figure 6(c)** depicts the temporal behavior of gaun, saturable loss, and pulse power. **Figure 6(d)** shows both the intensity and frequency profile. The resultant pulse duration is about 83 fs and the pulse is positively chirped. This can be explained by the nonlinear index of the gain and absorber medium. The nonlinear refraction in the gain medium originates from the linewidth enhancement, due to the enhancement of the spontaneous emission into a lasing mode by the high cavity quality factor of the microcavity in the vertical cavity structure of the semiconductor disk gain medium.

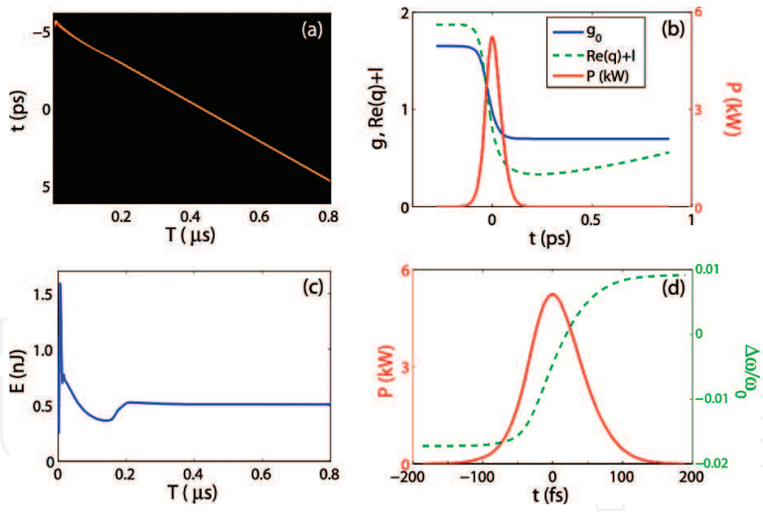

Figure 6. Evolution of pulse shape (a), power (b), duration (c), as well as frequency and power profile (d) in the GaN-based semiconductor disk laser (420 nm) with silica glass doped with Ag NPs. $D = 100$ fs^2.

Figures 7(a) and **(b)** show the dependences of pulse duration and energy on the cavity dispersion D. One can see that pulse shaping is unstable for the range of small dispersion (from $D = -150$ to 40 fs^2). The figure shows that the achievable shortest pulse duration is about 54.0 fs for negative dispersion of $D = -160$ fs^2 and about 55.3 fs for positive dispersion of $D = 50$ fs^2. For filling factor smaller than 6×10^{-3} due to the insufficient dynamic range of saturable loss, the mode-locked operation becomes unstable. For filling factor larger than 7×10^{-3}, the lasing itself is impossible due to the negative small signal net gain. For $f = 6 \times 10^{-3}$, $\tau_0 = 87.14$ fs and

$E = 0.69$ nJ, and for $f = 7 \times 10^{-3}$, $\tau_0 = 83.23$ fs and $E = 0.55$ nJ. These values are calculated for $D = -300$ fs^2.

In **Figures 7(c)** and **(d)**, we show the dependencies of pulse duration and energy on the beam area on the metal nanocomposite absorbers for both cases of positive and negative cavity dispersions, −300 and 300 fs^2.

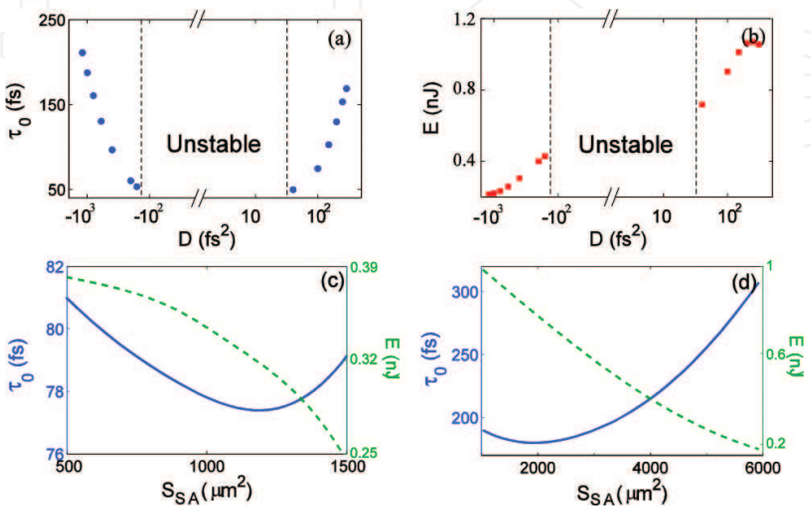

Figure 7. Dependencies of pulse duration (a) and energy (b) on the group delay dispersion D in the GaN-based semiconductor disk laser (420 nm) with silica composite doped with Ag NPs. Beam area on the saturable absorber composite is 1000 μm^2. Dependencies of pulse duration (c) and energy (d) on beam are on the silica glass doped with Ag NPs. In (c) $D = -300$ fs^2 and in (d) $D = 300$ fs^2.

In comparison with other well-established mode-locking elements such as semiconductor saturable absorber mirrors (SESAM), quantum dots, and carbon nanotubes, the operation range of metal nanocomposites as saturable absorber can be extended to much shorter wavelengths, down to the blue spectral range. Saturable absorbers in the visible spectral range can be realized by dyes dissolved in different solvents, but disadvantages such as maintaining a constant stream in the dye jet, temperature sensitivity, and long-term instability restrict their versatility. Different metal nanoparticle composites offer several advantages and allow the development of very compact and cheap mode-locking devices with tunable operation regions, extending from IR down to the blue spectral region. After the prediction of the possible application of metal nanocomposites for mode-locking of solid-state lasers [13] and semiconductor lasers [17], several groups successfully exploited nanoparticles for the generation of ultrashort pulses in mode-locked fiber lasers (see e.g. Refs. [29, 30], or solid-state lasers [31]).

5. Slow light by using metal nanoparticle composites

The possibility to reduce the group velocity of light significantly by various nonlinear effects has attracted much interest (see e.g., Refs. [32–35]). In this section, we show that metal nanocomposite materials can also significantly reduce the velocity of light. We assume that a metal nanocomposite is illuminated by a strong pump and a weak probe pulse with a

http://dx.doi.org/10.5772/67412

frequency slightly different from that of pump which is in the range near the SPR [see **Figure 8(a)**]. For convenience, we consider probe pulse with ps durations which is much longer than e-e interactions time τ_{ee} (see Section 2). In this case, the nonlinear dielectric function change of metal can approximately be written as follows [see Eq. (15)]:

$$\Delta\varepsilon_m(t) = \frac{\chi_m^{(3)}}{\tau_{ep}} \int_{-\infty}^{t} e^{-\frac{t-t'}{\tau_{ep}}} |A^{enh}(t')|^2 dt'. \tag{19}$$

As the slow light is a pulse propagating with a small group velocity, we have to study the propagation of a pulsed probe. Taking this into account, we write the amplitude of total enhanced field in metal NPs as

$$A^{enh}(t) = A_p^{enh} + A_{pr}^{enh}(t)e^{-i\Omega t}, \tag{20}$$

where $\Omega = \omega_{pr} - \omega_p$ is the difference between probe ω_{pr} and pump frequencies ω_p. The above equation can be rewritten by using the frequency-domain probe amplitude $A_{pr}^{enh}(\Omega)$:

$$A^{enh}(t) = A_p^{enh} + \int A_{pr}^{enh}(\Omega)e^{i\Omega t} d\Omega. \tag{21}$$

Assuming that the probe is much weaker than the pump, we obtain the dielectric functions of the metal at the pump and probe frequencies given by

$$\begin{aligned} \varepsilon_m(\omega_p) &= \varepsilon_{m0} + \chi_m^{(3)} |x_p A_p|^2, \\ \varepsilon_m(\omega_{pr}) &= \varepsilon_{m0} + \chi_m^{(3)} |x_p A_p|^2 \left(1 + \frac{1}{1 + i\Omega\tau_{ep}}\right), \end{aligned} \tag{22}$$

where $x_p = A_p^{enh}/A_p$ is the field enhancement factor for the pump depending on its intensity and is written by $x_p(\omega_p) = 3\varepsilon_h/[\varepsilon_m(\omega_p) + 2\varepsilon_h]$. We find the effective dielectric function for probe by using the Maxwell-Garnett formula. From the second equation in Eq. (22), we can expect that the effective dielectric function of metal nanocomposite has large dispersion in a narrow spectral range defined by τ_{ep}.

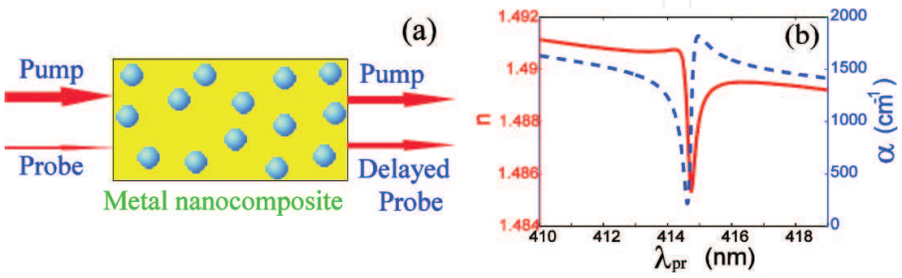

Figure 8. Scheme of slow-light device based on a metal-nanoparticle composite (a). The absorption coefficient (blue dashed line) and the effective index near the pump wavelength (red solid line) for the probe beam are shown in (b).

In **Figure 8(b)**, we show an example of the absorption spectrum and the effective refractive index for the probe in silica glass doped with Ag NPs. The steep increase of the effective index with the probe wavelength, as shown in the figure, leads to a large group index and strong slowing down of the probe wave.

For current applications, studying slow-light performance at telecommunication wavelengths is of particular importance. The plasmon resonance is shifted to a large extent for different shapes of the metallic NPs, with nanorods being particularly suitable to shift the plasmon resonance into the long wavelength range. Noble metals have extremely high inherent nonlinear susceptibilities at telecommunication wavelengths, e.g., for gold $\chi_m^{(3)} = -1.5 \times 10^{-11}$ m^2V^{-2}, which is 4 orders of magnitude higher than in the visible range [36]. Here, we solve the coupled propagation equations for the cw pump and the pulsed probe, to take into account the decrease of the pump intensity during the propagation due to the residual absorption and the change in the complex amplitude of probe, using the effective dielectric function calculated as explained above. The temporal profile of probe pulse is obtained by the Fourier transform.

Figure 9 shows typical incident and delayed pulses for a pump intensity of 6 MW/cm^2 at 1550 nm. We consider a TiO_2 film doped with gold nanorods with a diameter of 20 nm and a length of 66 nm with a surface plasmon resonance at 1540 nm. The propagation direction and polarization are the same for pump and probe beams. **Figure 9(a)** shows the evolution of probe pulse with propagation. Despite the saturation of the absorption for the pump, the output pump beam intensity is reduced down to 34 kW/cm^2 (not shown), which is about 200 times lower than that of input pump. The probe is sustained mainly by the coherent energy transfer from the pump and is attenuated by linear loss after the strong reduction of pump intensity. At a certain propagation length, the probe energy can become even larger than the incident energy. Here, gain peak for the probe arises already for quite low intensities. This can be seen in **Figure 9 (b)**: the probe peak intensity after 4 μm (green dash-dotted line) is 1.2 times larger than that of the incident pulse. For a propagation length of 5 μm, the fractional delay is roughly equal to 1.79, corresponding to a delay-bandwidth product of 2.68. As a central finding, the group velocity is 198 times smaller than the light velocity in vacuum. Because of the large inherent

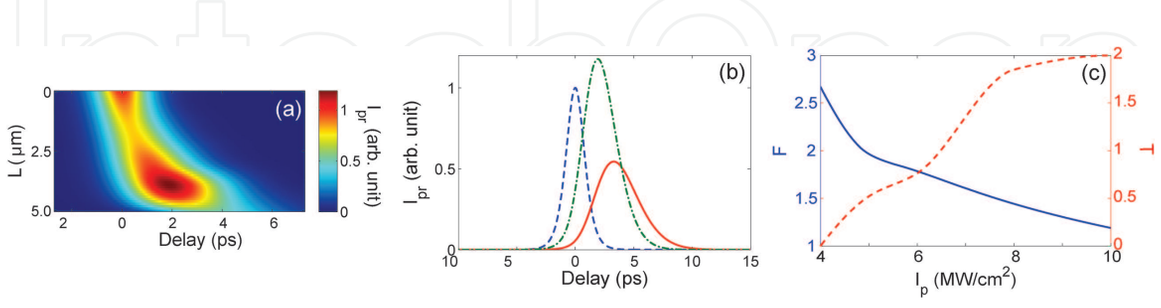

Figure 9. Slow light in TiO_2 film doped with Au nanorods, with a diameter of 20 nm and a length of 66 nm for pump intensity of 6 MW/cm^2 at 1550 nm. Filling factor is 2.5 × 10^{-2} and pulse duration is 1.85 ps. In (a) and (b), evolution of probe pulse and optical delay are shown, respectively. In (b), blue-dotted curve is the incident probe pulse, green dash-dotted and red solid curves are probe pulses for propagation lengths of 4 and 5 μm. In (c), we have shown the dependencies of fractional delay F (blue solid line), transmittance T (green-dotted line) on the pump intensity in TiO_2 film doped with Au nanorods at 1550 nm. The propagation length is 5 μm, the filling factor 5 × 10^{-2}, and the probe pulse duration 1.85 ps.

nonlinear susceptibility of gold in this wavelength range, the large fractional delay is achieved even with relatively low intensities of few MW/cm^2.

Figure 9(c) presents the dependence of fractional delay F (delay divided by the pulse duration of input probe) and transmittance T as functions of the pump intensity at 1550 nm. It can be seen that the fractional delay decreases as pump intensity increases, while the transmittance increases. In particular, for stronger pump, the transmittance for the probe can exceed unity due to amplification by an energy transfer from the pump. This feature constitutes a significant advantage compared to the conventional slow-light mechanism. **Figure 9(c)** shows that for a propagation length of 5 μm, a fractional delay in the range of 2 (corresponding to a delay-bandwidth product of 3) is predicted with a transmittance higher than 0.5.

Up to now, only a small number of experiments in different schemes have measured relative pulse delays exceeding these predictions. For comparison of results obtained with chip-compatible design, we refer to Ref. [32] with a fractional delay of 0.8 or to Ref. [33] with a value of 1.33. On the other hand, significantly larger fractional delays have been implemented by using cascaded microring resonators and photonic wire waveguides (but with relatively small probe transmission) [34] or by using double resonances of Cs atoms [35]. However, the numerical examples with a fractional delay of roughly two are not the physical limits of the method proposed here. Next, we will show that notably larger fractional delays can be realized using a modified setup.

The main drawback of the delay line in collinear configuration is due to the propagation length being limited by the attenuation of the pump. This can be circumvented using a transversely pumped setup as shown in **Figure 10(a)**, where the probe pulse is guided by the waveguide structure. The thickness of the film is 1 μm in this case, resulting in an attenuation of the pump intensity below 10%. Therefore, the pump intensity can be approximately considered to be constant. The other parameters are the same as for the case of **Figure 9** except the different pump intensity of 0.28 MW/cm^2. This value corresponds to a pump energy of 0.2 nJ for a 200 ps pump and a transverse waveguide width of 5 μm. Note that the polarization of pump and probe must be parallel due to the selective plasmon excitation for nonspherical NPs. **Figure 10(b)** shows the evolution of the probe pulse intensity normalized by the incident peak probe intensity. In this case, the peak intensity of the probe increases by a factor of 3.1 after propagation of 90 μm. For a more detailed presentation, in **Figure 10(c)**, we present the normalized probe pulses

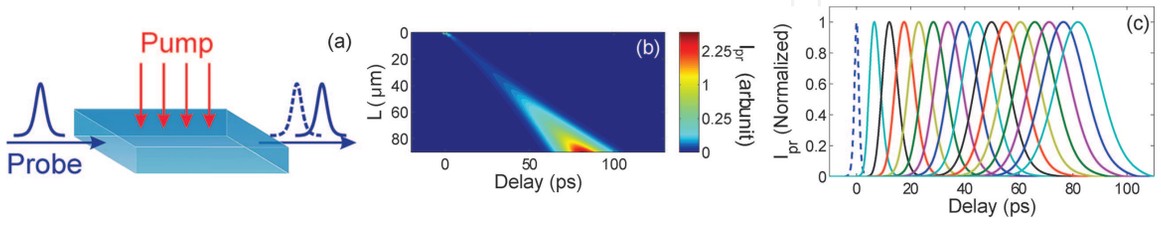

Figure 10. Delay for 1.85 ps probe pulse and pump intensity of 0.28 MW/cm^2 in TiO_2 film with a thickness of 1 μm in noncollinear configuration: (a) setup, (b) and (c) evolution of probe pulse. The remaining parameters are the same as in **Figure 9**. In (c), blue dashed curve is the incident pulse and solid curves are the delayed pulse profiles corresponding to propagation lengths L up to 90 μm with a step of 6 μm from the left to the right.

corresponding to propagation lengths up to 90 μm with a step of 6 μm. We predict a total fractional delay of about 43, with a delay-bandwidth product of 65 and a slowing down factor of 270. In this configuration, as the probe can be amplified, we have no principal limitation of the delay time; since with increasing propagation length, the delay time can be increased significantly which is only limited to the available pump source.

6. Conclusion

In this chapter, we presented a numerical method—the time-domain discrete-dipole approximation—for the calculation of the ultrafast nonlinear optical response of composites containing metal nanoparticles with different shapes. Based on the two-temperature model, an equation for the transient nonlinear response of metal nanocomposites is derived. This approach was applied for the study of the nonlinear refraction index and the transmittance of a thin fused silica glass layer doped with spherical nanoparticles and nanorods. The numerical results show that the total absorption coefficient exhibits strong saturation behavior near the plasmon resonance. The wavelength range of the saturated absorption can be significantly shifted in the whole ultraviolet, visible, and near-infrared spectral region by using metal NPs with nonspherical shapes. We have shown that the obtained results can be used for mode-locking of solid-state lasers and semiconductor lasers. In particular, in the short-wavelength range below 700 nm, useful saturable absorbers are still missing, but composites doped with metal NPs can enable the fabrication of new types of broadband mode-locking elements with a saturation intensity in the range of 10 MW/cm^2 and with an operation range from the near-IR up to the blue spectral range. As another example, we investigated theoretically a new slow-light mechanism based on composites doped with metal NPs. If two pulses with a frequency difference below the electron-phonon coupling rate propagate through such a composite, plasmon-induced oscillations of the nonlinear permittivity create a very high dispersion of the effective index for picoseconds-scale probe pulses, and correspondingly a strongly reduced group velocity. We have shown that utilizing these composites in a collinear setup reduced group velocities with a slow-down factor in the range of 200 and a fractional delay up to 2.5 for probe pulses with a few-ps duration can be implemented both at telecommunication wavelengths as well as in the optical range. Avoiding pump depletion, the relative delay can be significantly increased and a total fractional delay of 43 can be realized in a transversely pumped waveguide geometry.

Author details

Kwang-Hyon Kim[1], Anton Husakou[2] and Joachim Herrmann[2]*

*Address all correspondence to: jherrman@mbi-berlin.de

1 Institute of Lasers, State Academy of Sciences, Pyongyang, DPR Korea

2 Max Born Institute for Nonlinear Optics and Short Pulse Spectroscopy, Berlin, Germany

References

[1] Maier SA. Plasmonics: Fundamentals and Applications. Berlin: Springer; 2007.

[2] Zhang JZ, Noguez C. Plasmonic optical properties and applications of metal nanostructures. Plasmonics. 2008;**3**:127–150.

[3] Pelton M, Aizpurura J, Bryant G. Metal nanoparticle plasmonics. Laser Photon. Rev. 2008;**2**:136–159.

[4] Kelly KL, Coronado E, Zhao LL, Schatz GC. The optical properties of metal nanoparticles: the influence of size, shape, and dielectric environment. J. Phys. Chem. B. 2003;**107**:668–677.

[5] Sipe JE, Boyd RW. Nonlinear susceptibility of composite optical materials in Maxwell Garnett model. Phys. Rev. A. 1992;**46**:1614–1629.

[6] Hache F, Ricard D, Flytzanis C. Optical nonlinearities in small metal particle: surface-mediated resonance and quantum size effects. J. Opt. Soc. Am. B. 1986;**3**:1647–1655.

[7] Hache F, Ricard D, Flytzanis C. The optical Kerr effect in small metal particles and metal colloids: the case of gold. Appl. Phys. A. 1988;**47**:347–357.

[8] Palant B. Third-order nonlinear optical response of metal nanoparticles. In: Papadoulos MG et al, editor. Nonlinear Optical Properties of Matter. Berlin: Springer; 2006. pp. 461–508.

[9] Kim KH, Husakou A, Herrmann J. Linear and nonlinear optical characteristics of composites containing metal nanoparticles with different sizes and shapes. Opt. Express.2010; **18**:7488–7496.

[10] Kim KH, Yurkin MA. Time-domain discrete-dipole approximation for simulation of temporal response of plasmonic nanoparticles. Opt. Express.2015;**23**:15555–15564.

[11] Kim KH, Choe SH. Ultrafast nonlinear optical responses of dielectric composite materials containing metal nanoparticles with different sizes and shapes. Plasmonics (accepted). DOI: 10.1007/s11468-016-0335-x.

[12] Kim KH, Husakou A, Herrmann J. Saturable absorption in composites doped with metal nanoparticles. Opt. Express. 2010;**18**:21918–21925.

[13] Kim KH, Griebner U, Herrmann J. Theory of passive mode locking of solid-state lasers using metal nanocomposites as slow saturable absorbers. Opt. Lett. 2012;**37**:1490–1492.

[14] Tsen KT. Non-Equilibrium Dynamics of Semiconductors and Nanostructures. New York: CRC; 2005.

[15] Lysenko S, Jimenez J, Zhang G, Liu H. Nonlinear optical dynamics of glass-embedded silver nanoaprticles. J. Electron. Mater. 2006;**35**:1715–1721.

[16] Voisin C, Fatti ND, Christofilos D, Vallée F. Ultrafast electron dynamics and optical nonlinearities in metal nanoparticles. J. Phys. Chem. B. 2001;**105**:2264–2280.

[17] Kim KH, Griebner U, Herrmann J. Theory of passive mode-locking of semiconductor disk lasers in the blue spectral range by metal nanocomposites. Opt. Express. 2012;**20**:16174–16179.

[18] Bigot JY, Halté V, Merle JC, Daunois A. Electron dynamics in metallic nanoaprticles. Chem. Phys. 2000;**251**:181–203.

[19] Haus HA. Mode-locking of lasers. IEEE J. Sel. Top. Quantum Electron. 2000;**6**:1173–1185.

[20] Walsh BM, Barnes NP, Bartolo BD. Branching ratios, cross sections, and radiative lifetimes of rare earth ions in solids: application to Tm^{3+} and Ho^{3+} ions in LiYF4. J. Appl. Phys. 1998;**83**:2772–2787.

[21] Walsh BM, Barnes NP, Petros M, Yu J, Singh UN. Spectroscopy and modeling of solid state lanthanide lasers: application to trivalent Tm^{3+} and Ho^{3+} in $YLiF_4$ and $LuLiF_4$. J. Appl. Phys. 2004;**95**:3255–3271.

[22] Herrmann J, Müller M. Hidden mechanism for mode locking solid-state lasers by use of slow off-resonant saturable absorbers. Opt. Lett. 1995;**20**:994–996.

[23] Kaertner FX, Au JA der, Keller U. Soliton mode-locking with saturable absorbers, IEEE J. Sel. Top. Quantum Electron. 1996;**2**:540–556.

[24] Paschotta R, Keller U. Passive mode locking with slow saturable absorbers. Appl. Phys. B. 2001;**73**:653–662.

[25] Keller U. Ultrafast solid-state laser oscillators: a success story for the last 20 years with no end in sight. Appl. Phys. B. 2010;**100**:15–28.

[26] Saarinen EJ, Herda R, Okhotnikov OG . Dynamics of pulse formation in mode-locked semiconductor disk lasers. J. Opt. Soc. Am. B. 2007;**24**:2784–2790.

[27] Lu TC, Chu JT, Chu SW, Chen SW, Cheng BS, Kuo HC, Wang SC. Temperature dependent gain characteristics in GaN-based vertical-cavity surface-emitting lasers. Opt. Express. 2009;**17**:20149–20154.

[28] Smetanin IV, Vasil'ev PP, Boiko DL. Theory of the ultrafast mode-locked GaN lasers in a large-signal regime. Opt. Express. 2011;**19**:17114–17120.

[29] Kang Z, Xu Y, Zhang L, Jia Z, Liu L, Zhao D, et al. Passively mode-locking induced by gold nanorods in erbium-doped fiber lasers. Appl. Phys. Lett. 2013;**103**:041105.

[30] Wang XD, et al. Microfiber-based gold nanorods as saturable absorbers for femtosecond pulse generation in a fiber laser. Appl. Phys. Lett.2014;**105**:161074.

[31] Huang HT, et al. Gold nanorods as single and combined saturable absorbers for a high-energy q-switched Nd:YAG solid-sate laser. IEEE Photon. J.. 2015;**7**:4501210.

[32] Wu B, Hulbert JF, Lunt EJ, Hurd K, Hawkins AR, Schmidt H. Slow light on a chip via atomic quantum state control. Nature Photon. 2010;**4**:776–779.

http://dx.doi.org/10.5772/67412

[33] Okawachi Y, Foster MA, Sharping JE, Gaeta AL, Xu Q, Lipson M. All-optical slow-light on a photonic chip. Opt. Express. 2006;**14**:2317–2322.

[34] Xia F, Sekaric L, Vlasov Y. Ultracompact optical buffers on a silicon chip. Nature Photon. 2007;**1**:65–71.

[35] Camacho RM, Pack MV, Howell JC, Schweinsberg A, Boyd RW. Wide-bandwidth, tunable, multiple-pulse-width optical delays using slow light in Cesiumvapor. Phys. Rev. Lett. 2007;**98**:153601.

[36] Falcao-Filho EL, Barbosa-Silva R, Sobral-Filho RG, Brito-Silva AM, Galembeck A, Araujo CB. High-order nonlinearity of silica-gold nanoshells in chloroform at 1560 nm. Opt. Express. 2010;**18**:21636–21344.

IntechOpen